Journal of Controlled Release 358 (2023) 116–127

Contents lists available at ScienceDirect

Journal of Controlled Release

journal homepage: www.elsevier.com/locate/jconrel

Changes in local tissue microenvironment in response to subcutaneous long-acting delivery of tenofovir alafenamide in rats and non-human primates

Fernanda P. Pons-Faudoa [a], Nicola Di Trani [a], Simone Capuani [a,b], Nathanael Hernandez [a], Anthony M. Wood [a], Bharti Nehete [c], Jean Niles [d], Kathryn A. Shelton [c], Sarah Kezar [c], Lane R. Bushman [e], Corrine Ying Xuan Chua [a], Michael M. Ittmann [f], Peter L. Anderson [e], Pramod N. Nehete [c,g], Roberto C. Arduino [h], Joan E. Nichols [d], Alessandro Grattoni [a,i,j,*]

[a] Department of Nanomedicine, Houston Methodist Research Institute, Houston, TX 77030, USA
[b] University of Chinese Academy of Science (UCAS), 19 Yuquan Road, Beijing 100049, China
[c] Department of Comparative Medicine, Michael E. Keeling Center for Comparative Medicine and Research, MD Anderson Cancer Center, Bastrop, TX 78602, USA
[d] Department of Surgery, Houston Methodist Hospital, Houston, TX 77030, United States of America
[e] Deparment of Pharmaceutical Sciences, Skaggs School of Pharmacy and Pharmaceutical Sciences, University of Colorado- Anschutz Medical Campus, Aurora, CO 80045, USA
[f] Department of Pathology and Immunology, Baylor College of Medicine, Houston, TX 77030, USA
[g] The University of Texas Graduate School of Biomedical Sciences at Houston, Houston, TX 77030, USA
[h] Division of Infectious Diseases, Department of Internal Medicine, McGovern Medical School at The University of Texas Health Science Center, Houston, TX 77030, USA
[i] Department of Surgery, Houston Methodist Research Institute, Houston, TX 77030, USA
[j] Department of Radiation Oncology, Houston Methodist Research Institute, Houston, TX 77030, USA

ARTICLE INFO

Keywords:
Long acting drug delivery
Subcutaneous implants
Tenofovir alafenamide
Foreign body response
Immune microenvironment

ABSTRACT

Several implantable long-acting (LA) delivery systems have been developed for sustained subcutaneous administration of tenofovir alafenamide (TAF), a potent and effective nucleotide reverse transcriptase inhibitor used for HIV pre-exposure prophylaxis (PrEP). LA platforms aim to address the lack of adherence to oral regimens, which has impaired PrEP efficacy. Despite extensive investigations in this field, tissue response to sustained subcutaneous TAF delivery remains to be elucidated as contrasting preclinical results have been reported in the literature. To this end, here we studied the local foreign body response (FBR) to sustained subdermal delivery of three forms of TAF, namely TAF free base (TAF_{fb}), TAF fumarate salt (TAF_{fs}), and TAF_{fb} with urocanic acid (TAF-UA). Sustained constant drug release was achieved via titanium–silicon carbide nanofluidic implants previously shown to be bioinert. The analysis was conducted in both Sprague-Dawley (SD) rats and rhesus macaques over 1.5 and 3 months, respectively. While visual observation did not reveal abnormal adverse tissue reaction at the implantation site, histopathology and Imaging Mass Cytometry (IMC) analyses exposed a local chronic inflammatory response to TAF. In rats, UA mitigated foreign body response to TAF in a concentration-dependent manner. This was not observed in macaques where TAF_{fb} was better tolerated than TAF_{fs} and TAF-UA. Notably, the level of FBR was tightly correlated with local TAF tissue concentration. Further, regardless of the degree of FBR, the fibrotic capsule (FC) surrounding the implants did not interfere with drug diffusion and systemic delivery, as evidenced by TAF PK results and fluorescence recovery after photobleaching (FRAP).

1. Introduction

The approval of antiretrovirals (ARVs) for human immunodeficiency virus (HIV) pre-exposure prophylaxis (PrEP) in 2012 has contributed to a reduction in new infections worldwide. However, according to the United Nations, 1.5 million people were estimated to have become newly infected in 2021 [1]. Current FDA-approved oral HIV PrEP contains tenofovir (TFV) prodrugs, tenofovir disoproxil fumarate (TDF) or

* Corresponding author at: Department of Nanomedicine, Houston Methodist Research Institute, Houston, TX 77030, USA.
E-mail address: agrattoni@houstonmethodist.org (A. Grattoni).

https://doi.org/10.1016/j.jconrel.2023.04.037
Received 28 March 2023; Received in revised form 19 April 2023; Accepted 23 April 2023
Available online 29 April 2023

tenofovir alafenamide (TAF), in combination with emtricitabine (FTC) in a pill. While pharmacologically these regimens offer high protection against infection, clinical efficacy has been limited by lack of adherence and consequently a decrease in tenofovir diphosphate (TFV-DP) concentration inside target peripheral blood mononuclear cells (PBMCs) [2,3]. This was documented in clinical trials with men who have sex with men, where a decrease in protection was shown to occur with missed doses [4].

To obviate adherence issues, increase PrEP efficacy, and broaden its access and uptake, several long-acting (LA) delivery technologies have been developed in injectable or implantable forms, capable of constantly administering PrEP for months to years, uninterrupted [5–7]. In this context, high potency ARVs have received particular interest to enable single-drug LA systems with small injection volumes for injectables or drug reservoir size for minimally-invasive and discreet implants [8,9]. Given the potency and safety advantages of TAF compared to TDF, numerous LA TAF strategies have been evaluated in preclinical studies including biodegradable or non-biodegradable polymeric implants, transcutaneously refillable devices, and an osmotic pump. Clinically, LA TAF polymeric implants are being investigated in the CAPRISA 018 phase I/II clinical trial for HIV PrEP in women [10].

Notably, contrasting results have been reported regarding local tissue tolerability of sustained subdermal TAF administration. Drawing a cohesive picture from these findings is challenging due to differences in animal models, implant materials and properties, TAF doses, and formulations used. In this study, we performed a comparative assessment of tolerability, local tissue response, and immune cell infiltration in response to sustained subcutaneous administration of TAF. Three forms of TAF were used. TAF fumarate salt and TAF free base were employed given their adoption in LA systems, including the implants used in the CAPRISA clinical trial. The third formulation consisted of TAF free base formulated with *trans*-urocanic acid (TAF-UA), which was previously shown to enhance TAF stability by decreasing its hydrolytic degradation [11]. The three formulations were released from non-degradable bioinert nanofluidic implants consisting of a titanium reservoir and a silicon carbide-coated nanochannel membrane. In a survival study, the investigation was executed in rats and rhesus macaques, with animals receiving two nanofluidic devices each, implanted in the dorsum contralaterally: 1) one implant loaded with one form of TAF, and 2) one implant loaded with vehicle (PBS) as no-drug control.

2. Materials and methods

2.1. Implant assembly

For in vivo rat experiments, implants (20 mm × 13 mm × 4.5 mm) were 3D printed in biocompatible photopolymer resin using a stereolithography printer (SLA, Formlabs 3D). For in vivo nonhuman primate (NHP) experiments, implants with similar dimensions were machined in medical-grade titanium at the Machine Shop of the Houston Methodist Research Institute (HMRI). The nanofluidic membrane (6 mm × 6 mm × 0.4 mm) was mounted within the membrane holder in the implant shell (membrane shell). The membrane was glued with biocompatible UV Epoxy (MED-OG116-31, Epotek) as previously described [12–14]. Implants were loaded with the respective drug: *trans*-urocanic acid, tenofovir alafenamide free base (TAF_{fb}, GS 7340, Gilead Sciences Inc.), tenofovir alafenamide fumarate (TAF_{fs}, GS 7340-03, Gilead Sciences Inc.) and left empty for the control group. Resin implant shells were hermetically sealed with the same uncured photopolymer resin and cured under UV light. Titanium implant shells were welded using arc welding as previously described [12,14]. Implants were primed with 1× phosphate buffered saline under vacuum in aseptic conditions as previously described [12,14]. Implants were gamma sterilized (VPTRad) in a container, which was kept sealed until implantation.

2.2. Rodent care and implantation procedure

All rodent experiments were conducted at the Comparative Medicine Program, HMRI, Houston, TX. All animal experiments were carried out according to the provisions of the Animal Welfare Act, PHS Animal Welfare Policy, and the principles of the NIH Guide for the Care and Use of Laboratory Animals. The humane use of animals in research and all procedures detailed in the Institutional Animal Care and Use Committee (IACUC) protocol number AUP-0620-0040 were approved by the IACUC at HMRI. 10-week-old male Sprague Dawley rats ($n = 16$) were purchased from Charles River (Houston, TX, USA) and used in the study. Animals were housed under standard conditions and had ad libitum access to water and a standard laboratory diet.

Carprofen wafers were administered 1- and 2-days pre-surgery, on implantation day, and 1- and 2-days post-surgery. Buprenorphine SR (1 mg/kg) was administered on implantation day. A small skin incision in the subscapular region was made perpendicular to the vertebral column in the anesthetized animal. Caudal blunt dissection within the incision line created a subcutaneous pocket enough for implant placement. The implant was placed in the subcutaneous pocket with the nanofluidic membrane facing the dermis. A splash block of bupivacaine (5 mg/kg/day) was delivered, and the skin was closed with staples. Implant measurements (length, width, and height) were performed weekly for up to 6 weeks using a caliper. Pictures were taken weekly.

2.3. Implant removal and histopathologic assessment

The skin within a 2 cm margin surrounding the implant was excised from euthanized rodents. The implant was retrieved with a small incision in the fibrotic capsule (FC). A 3D-printed implant made with a flexible polymer and identical dimensions was placed within the FC as a placeholder for tissue fixation. The tissue was fixed in 10% buffered formalin and stored in 70% ethanol. The tissue was sectioned, and the placeholder implant removed before histological analysis. Tissues surrounding the implant site were then embedded in paraffin, cut into 5 um sections and stained with H&E staining at the Research Pathology Core HMRI, Houston, TX, USA.

Semiquantitative histopathological assessment of inflammatory response to a foreign body was evaluated in accordance with the inflammation scoring system presented in Su et al. [15] which was adopted from a published standard [16] as previously described [12]. Two board-certified pathologists from independent institutions performed the blinded histopathological assessment of the samples. The scores reported by each pathologist were averaged per implant (Table S1, Supporting Information). Then, the total histological characteristic scores were reported per group as the average of the sum of all histological scores of all implants. The reactivity grade for each implant group was computed using Eq. (1) from Su et al. [15] and the average placebo-adjusted implant reactivity score (S_{pair}) was calculated by subtracting the result obtained for the control from treatment groups (TAF_{fb}, UA, TAF-UA, and TAF_{fs}). The Spair classification used in Su et al. [15] and published standard was adopted: minimal to no reaction ($0.0 < S_{pair} < 2.9$), slight reaction ($3.0 < S_{pair} < 8.9$), moderate reaction ($9.0 < S_{pair} < 15.0$), severe reaction ($S_{pair} > 15.1$).

Assessment of FC surrounding implant, collagen density, and blood vessel count were executed distinctly for the portions of tissues adjacent to the membrane as well as for the opposite side of implants. Fibrotic capsule thickness was measured with Image J software using Masson trichrome images of the full FC in ten areas on the side in contact with the membrane and the opposite side. Collagen density was assessed with multiple Masson trichrome images of 40× magnification of the FC in contact with the membrane and opposite side using MATLAB® software. Blood vessel lumens were counted with Image J software using full H&E images of FC in contact with the membrane and opposite side.

2.4. Macaque care and implantation procedure

All animal procedures were conducted at the AAALAC-I accredited Michale E. Keeling Center for Comparative Medicine and Research, The University of Texas MD Anderson Cancer Center (UTMDACC), Bastrop, TX. All animal experiments were carried out according to the provisions of the Animal Welfare Policy, and the principles of the NIH Guide for the Care and Use of Laboratory Animals. All procedures were approved by the Institutional Animal Care and Use Committee (IACUC) at UTMDACC, which has an Animal Welfare Assurance on file with the Office of Laboratory Animal Welfare. Animal Care and Use Form (ACUF) #00001749-RN00. Indian rhesus macaques (*Macaca mulatta*; $n = 12$; 2 males, and 10 females) of 3 years and 2–5 kg bred at this facility were used in the study. All procedures were performed under anesthesia with ketamine (10 mg/kg, intramuscular) and inhaled isoflurane (1 mL per 10 lb). All animals were pair-housed and had access to clean, fresh water at all times and a standard laboratory diet.

An approximately 1 cm dorsal skin incision was made on the left and right lateral side of the thoracic spine. Blunt dissection was used to make a subcutaneous pocket ventrally about 5 cm deep. The control and treatment (TAF, TAF fumarate, or TAF-UA) implants were placed on the left and right subcutaneous pockets, respectively, with the membrane facing the body. A simple interrupted tacking suture of 4-0 polydioxanone (PDS) was placed in the subcutaneous tissue to help close the dead space and continued intradermally to close the skin. All animals received a single 50,000 U/kg perioperative penicillin G benzathine/penicillin G procaine (Combi-Pen) injection and subcutaneous once-daily meloxicam (0.2 mg/kg on day 1 and 0.1 mg/kg on days 2 and 3) for postsurgical pain. Implant measurements (length, width, and height) were performed on days 1, 2, 3, 7 and weekly for up to 3 months using a caliper. Pictures and clinical observations were recorded with each measurement.

2.5. Implant removal and histopathologic assessment NHP

Animals were anesthetized and implants with surrounding FCs were retrieved with a small incision in the skin, which was then closed with a simple interrupted tacking suture of 4-0 PDS. A 3D printed implant made with flexible polymer and identical dimensions was placed within the FC as a placeholder for tissue fixation. The tissue was fixed in 10% buffered formalin and stored in 70% ethanol. The tissue was sectioned, and the placeholder implant removed prior to histological analysis. Tissues surrounding the implant site were then embedded in paraffin, cut into 5 μm sections and stained with H&E staining at the Research Pathology Core HMRI, Houston, TX, USA. Histopathological was performed following the same procedure described for rats in Section 2.3.

Fluorescence recovery after photobleaching (FRAP) analysis was performed on the FCs to assess drug diffusion, in accordance with our previous study [6]. Briefly, formalin-fixed FC tissue samples ($n = 2$ per group) and subcutaneous tissue samples ($n = 2$) were placed in a solution of 2 mg/mL FITC (Invitrogen) in DMEM/F12 media (Gibco) and incubated overnight at 4°C. Samples were removed from solution and placed in microscope chamber slides (Ibidi). FRAP measurements were performed with the Olympus Fluoview 3000 confocal microscope equipped with a 10× objective and a 488 nm laser on three fields of view (FOV) per sample. The method was validated with measurements of the FITC solution alone ($n = 3$). For each FOV, three pre-bleaching images were collected at low laser intensity (1%). Afterwards, bleaching was achieved by exposing a circular area (100 pixels or 248 μm diameter) at 100% laser intensity for 60 s. Finally, fluorescence recovery was assessed by acquiring images of the bleached area at low laser intensity for 15 min (10 images/min).

The data was analyzed with the Olympus cellSens software to obtain the characteristic diffusion time τ. This value, along with the radius of the bleached area, ω, is used to calculate the diffusion coefficient, D, according to the following equation [17]:

$$D = \frac{\omega^2}{4\tau}$$

2.6. Imaging mass cytometry (IMC)

IMC analysis was conducted at the ImmunoMonitoring Core (Houston Methodist Research Institute, Houston, TX). Antibodies were conjugated with metals following the Fluidigm protocol as previously mentioned [18]. Tissue sections were kept at 60°C overnight followed by deparaffinization in xylene and rehydration in alcohol gradients (absolute ethanol, absolute ethanol: deionized water 90:10, 80:20, 70:30, 50:50, 0:100) for 10 min each. Epitope retrieval was performed in a water bath at 95°C in Tris-Tween 20 buffer pH 9 for 20 min. Sections were blocked with 3% BSA in tris-buffered saline, followed by staining overnight at 4°C with markers and nuclear staining with Cell-ID Intercalator (Fluidigm). Twenty one markers were used to map immune cell populations, the panel included: cell surface receptors (CD45, CD4, CD8, CD20, CD3), signaling mediators (pSTAT1, pSTAT3), markers of cell activation (NFkB, tBet, HLA-DR, MPO), blood vessels (VCAM-, αSMA), fibrosis (collagen), macrophage differentiation to M1 or M2 cells (CD68, CD163, Arg1, NOS2), T cell regulatory (Foxp3), activated CD8 T cells (Granzyme B), and exhausted T cells (PD-1). After staining, slides were air-dried and ablated with Hyperion (Fluidigm) for data acquisition. Data were segmented by ilastik and CellProfiler. Histology topography cytometry analysis toolbox (HistoCAT) and R scripts were used to quantify cell number and generate tSNE plots [19]. Analysis was performed on 2 ROI/sample and $n = 1$/group for a total of $n = 2$ ROI/group.

2.7. Drug residual

Upon explanation, the implants were stored at −80°C to preserve residual drug. Residual drug retrieval was performed as previously described [12]. Briefly, a hole was drilled on the outermost corner on the back of the implant. The implants were placed in 50 mL conical tubes with 5 mL of dimethyl sulfoxide (DMSO). Each implant was flushed using a 19-gauge needle with DMSO from the sink solution. Drug residual from within the implant were analyzed from the 5 mL DMSO sink solution. Samples were diluted 200 times in PBS and transferred to 0.2 μm nylon centrifugal filter and centrifuged at 500 ×*g* for 8 min at room temperature. HPLC analysis of TAF was performed as previously described [11,12].

2.8. Blood collection and plasma and PBMC samples preparation

All animals had blood draws to assess plasma TAF and tenofovir (TFV) concentrations and intracellular tenofovir diphosphate (TFV-DP) concentrations in peripheral blood mononuclear cells (PBMC). Blood collection and sample preparation were performed as previously described [12]. Blood was collected in EDTA-coated vacutainer tubes before implantation; on days 1, 2, 3, 7, 14 and on months 1, 2, and 3. Plasma was separated from blood by centrifugation at 1200 ×*g* for 10 min at 4°C and stored at −80°C until analysis. The remaining blood was used for PBMC separation by standard Ficoll-Hypaque centrifugation. Cell viability was >95%. After cells were counted, they were pelleted by centrifugation at 400 ×*g* for 10 min, resuspended in 500 μL of cold 70% methanol per 30% water, and stored at −80°C until further use. Intracellular TFV-DP concentrations in PBMC were quantified using a previously described and validated liquid chromatographic-tandem mass spectrometric (LC-MS/MS) analysis [20,21]. The assay was linear from 5 to 6000 fmol per sample. Plasma TAF and TFV concentrations were quantified using a previously described LC-MS/MS assay [20].

2.9. Statistical analysis

Data are presented as mean ± SD. One-way ANOVA corrected with

Brown-Forsythe and Welch was used to compare fibrotic thickness with treatment groups, and histological score with treatment groups. Outliers were identified via ROUT method with Q = 0.1%. Statistical significance was defined as two-tailed $p < 0.05$ for all tests. All statistical analyses were performed with GraphPad Prism 9 (version 9.3.1; GraphPad Software, Inc., La Jolla, CA).

3. Results

3.1. Local tissue response in rats

We previously showed that, by lowering and maintaining the implant drug reservoir pH to 5.3, *trans*-UA can extend the stability of TAF in the implant environment for several months. In vivo, *trans*-UA is converted in its *cis*-form (*cis*-UA), which was shown to have immunomodulatory properties and to reduce inflammation in the context of various diseases [22] as well as in tissue allo-transplantation in rodents [23]. Here we aimed at investigating UA's role on modulating the FBR in response to implants and 6-weeks sustained TAF subdermal delivery. Male SD rats ($n = 4$ per group) were subcutaneously implanted with nanofluidic devices loaded with either TAF-UA_{hi} (TAF:UA ratio 1:1), TAF-UA_{lo} (TAF:UA ratio 10:1), UA, and PBS (Fig. 1a–d). Non-invasive visual assessment of the implantation site showed no sign of redness and erythema throughout the study (Fig. 1a–d). However, clinical observations reported induration in four of sixteen implants. Specifically, this was observed in two TAF-UA_{hi} and two TAF-UA_{lo} on the 3rd and 4th week post-implantation, respectively. Potential swelling was monitored weekly up to week 6 post-implantation by non-invasive measurements of tissue thickness at the implantation site via a caliper. Measurements were performed along virtual x- and y-axes, corresponding to the length and width of implants, respectively and parallel to the skin (Fig. 1e). Measurements orthogonal to the skin (z-axis) were also collected. Changes were normalized to value taken on first measurement (week 1), obtaining ΔT_x, ΔT_y, ΔT_z. ΔT_x and ΔT_y were subsequently averaged for each time point and normalized to the first measurement, obtaining $\Delta T_{x\text{-}y}$ (Fig. 1f–j). In average, a longitudinal increase in $\Delta T_{x\text{-}y}$ was observed for the TAF-UA_{hi} and TAF-UA_{lo} groups. This was not visible for the PBS and UA groups where tissue thickness levels remained stable throughout the analysis. At week 6, mean $\Delta T_{x\text{-}y}$ for control PBS, UA, TAF-UA_{hi}, and TAF-UA_{lo} were 0.19 ± 0.13, −0.057 ± 0.20, 0.89 ± 0.31, and 0.63 ± 0.27 mm, respectively. Statistical significance was observed between the overall means of TAF-UA_{lo} and UA groups ($p = 0.014$), TAF-UA_{hi} and PBS ($p = 0.024$), and TAF-UA_{hi} and UA groups ($p = 0.0035$). Similar observations were noted for tissue thickening along the z-axis: while control PBS and UA maintained a mean depth ΔT_z of 0.46 ± 0.15, 0.075 ± 0.23 mm, both TAF-UA_{hi} and TAF-UA_{lo} groups showed an increasing ΔT_z trend over the 6 weeks study, with substantially larger mean ΔT_z values (at week 6) of 1.4 ± 0.59 and 1.8 ± 0.67, respectively (Fig. 1k–o). Statistical significance was detected between the overall means of PBS and UA groups ($p = 0.016$), TAF-UA_{lo} and UA groups ($p = 0.030$), TAF-UA_{lo} and PBS groups ($p = 0.045$) and TAF-UA_{hi} and UA groups ($p = 0.034$).

With the exception of the PBS group, H&E histology of tissue surrounding the implants showed a notable difference in fibrotic capsule (FC) thickness in tissue adjacent the nanofluidic membrane, indicated as "M" if Fig. 2, with respect to the tissue on the opposite side of implants, denoted as "O" (Fig. 2a–i): this difference was particularly remarkable for TAF-UA_{hi} and TAF-UA_{lo}, indicating the inflammatory effect of TAF in tissues subject to sustained exposure to the drug. Thicknesses (mean ± SD, μm) of FCs in contact with membrane were: PBS (97.81 ± 23.80), UA (176.39 ± 128.64), TAF-UA_{hi} (1333.04 ± 1432.74) and TAF-UA_{lo} (1797.59 ± 1536.95). Fibrotic tissue thicknesses on the opposite side of implants were: UA (93.18 ± 21.74), TAF-UA_{hi} (147.59 ± 71.98) TAF-UA_{lo} (97.14 ± 29.17) and PBS (82.32 ± 23.07) (Fig. 2i). Statistical significance was observed for FC thickness between the membrane side and the opposite side for each group except PBS: UA ($p = 0.0064$), TAF-

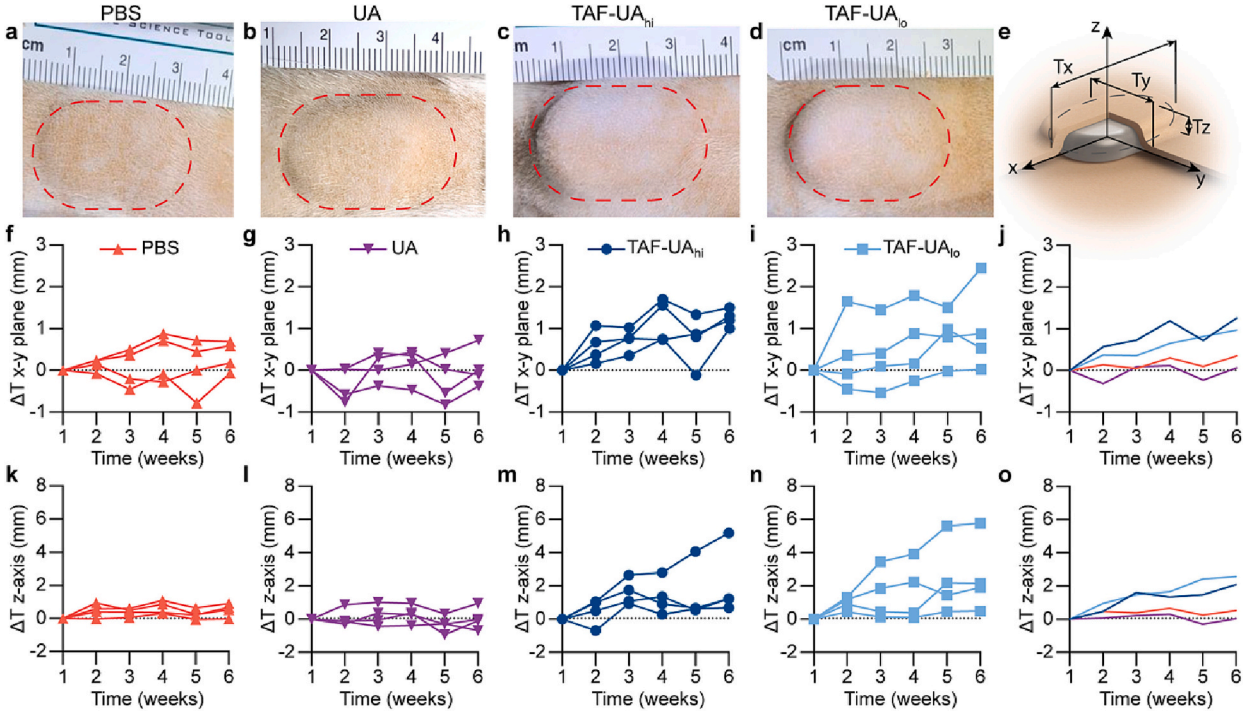

Fig. 1. Urocanic acid (UA) contribution to reduce local inflammation from TAF-releasing nanofluidic implant. Representative image of (a) control PBS, (b) UA, (c) TAF-UA_{hi} and (d) TAF-UA_{lo} nanofluidic implants in Sprague-Dawley rats at 6 weeks. (e) Schematics of subcutaneous implant illustrating the measurements of tissue thickness along the x-, y- and z-axes. Change in implant thickness ($\Delta T_{x\text{-}y}$) averaged with respect to length and width (x-y plane) throughout 6 weeks in (f) PBS, (g) UA, (h) TAF-UA_{hi}, (i) TAF-UA_{lo} and (j) comparison of 4 groups. Change in implantation site thickness along the z-axis (ΔT_z) throughout 6 weeks in (k) PBS, (l) UA, (m) TAF-UA_{hi}, (n) TAF-UA_{lo} and (o) comparison of 4 groups.

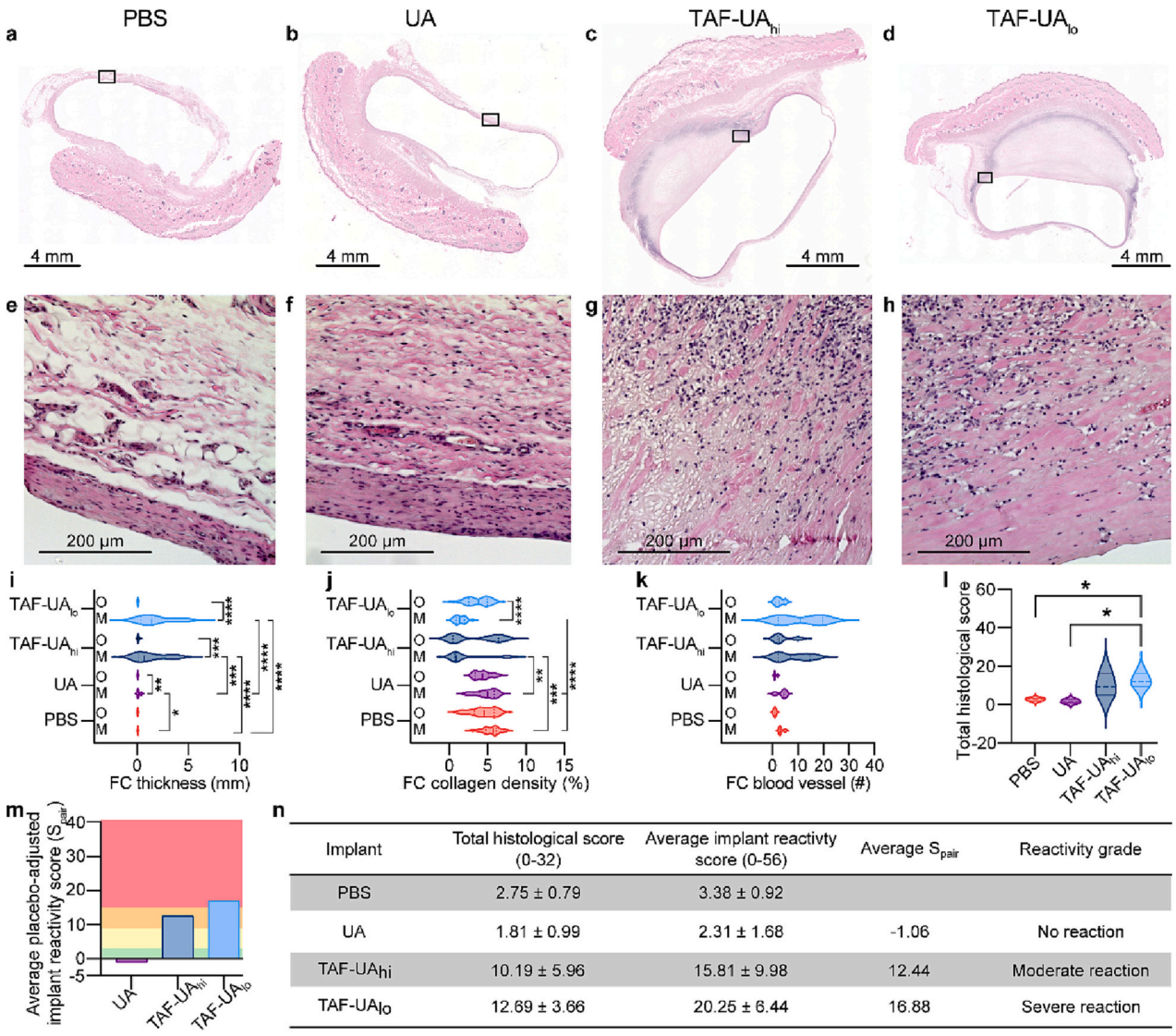

n

Implant	Total histological score (0-32)	Average implant reactivty score (0-56)	Average S_{pair}	Reactivity grade
PBS	2.75 ± 0.79	3.38 ± 0.92		
UA	1.81 ± 0.99	2.31 ± 1.68	-1.06	No reaction
TAF-UA$_{hi}$	10.19 ± 5.96	15.81 ± 9.98	12.44	Moderate reaction
TAF-UA$_{lo}$	12.69 ± 3.66	20.25 ± 6.44	16.88	Severe reaction

Fig. 2. H&E staining of fibrotic capsules (FC) harvested after 6-weeks of implantation for implants loaded with (a) PBS, (b) UA, (c) TAF-UA$_{hi}$ and (d) TAF-UA$_{lo}$, and corresponding magnification of rectangular areas for (e) PBS, (f) UA, (g) TAF-UA$_{hi}$ and (h) TAF-UA$_{lo}$. Comparison of (i) FC thickness, (j) collagen percentage in FC area and (k) blood vessel quantity in FC for tissues adjacent the membrane (M) and on the opposite side of implants (O). (l) Evaluation of total histological scores between PBS, UA, TAF-UA$_{hi}$ and TAF-UA$_{lo}$ groups. (m) Assessment of average S_{pair} reactivity grade between UA, TAF-UA$_{hi}$ and TAF-UA$_{lo}$. S_{pair} values: 0.0–2.9, 3.0–8.9, 9.0–15.0, and > 15.1 colored as green (no reaction), yellow (slight reaction), orange (moderate reaction) and red (severe reaction). (n) Table with histopathological scoring in all 4 groups. Data presented as mean ± SD. (For interpretation of the references to colour in this figure legend, the reader is referred to the web version of this article.)

UA$_{hi}$ ($p = 0.0002$), TAF-UA$_{lo}$ ($p < 0.0001$), and PBS ($p = 0.11$). Additionally, statistical significance was observed for tissue adjacent the membranes between all groups except TAF-UA$_{hi}$ with TAF-UA$_{lo}$ ($p = 0.99$).

Masson Trichrome staining highlighted differences in collagen density (mean ± SD, %) in FCs (Fig. 2j). Collagen density was similar for both PBS and UA groups on both membrane and opposite side of implants, which values were: PBS membrane side (5.50 ± 1.05), PBS opposite side (4.41 ± 1.58), UA membrane side (4.85 ± 1.29) and UA opposite side (4.38 ± 1.03). In TAF-UA$_{lo}$ statistically significant differences were noted between membrane and opposite implant side ($p < 0.0001$). Additionally, both TAF-UA$_{lo}$ and TAF-UA$_{hi}$ displayed significant collagen density differences with respect to PBS and UA groups for tissues adjacent to the membranes. Collectively, the lower collagen density observed in FC in TAF groups may be ascribed to the effect of drug-induced metalloprotease degradation of tissue causing a reduction in collagen density. Differences between TAF-UA$_{lo}$ and TAF-UA$_{hi}$ suggest that UA mitigates this effect in a concentration-dependent manner.

The number of blood vessel lumens (mean ± SD, count) within FCs in contact with membrane were: PBS (3.5 ± 1), UA (3.75 ± 1.89), TAF-UA$_{hi}$ (8 ± 6.68) and TAF-UA$_{lo}$ (11 ± 9.13) (Fig. 2k). None of the groups reported statistical significance between them. Additionally, no statistical significance was found between the membrane and opposite sides of implants in PBS (1 ± 0, $p = 0.13$), UA (1.25 ± 0.5, $p > 0.99$), TAF-UA$_{hi}$ (4.25 ± 3.86, $p > 0.99$) and TAF-UA$_{lo}$ (2.75 ± 1.71, $p > 0.99$) (Fig. 2k). However, for TAF groups the distribution of blood vessel count was substantially wider adjacent to the membrane as compared to the opposite implant side. This is consistent with increased angiogenesis in correspondence to increased tissue inflammation.

Tissues in contact with the implants were analyzed and scored by 2 board-certified pathologists blind to the treatment groups to quantify foreign-body reaction. Quantification was based on the presence of polymorphonuclear cells, lymphocytes, plasma cells, macrophages,

giant cells, necrosis, capsule thickness, and tissue infiltrate (Supplementary Table S1). PBS control and UA groups received similar pathology scores, 2.75 ± 0.79 and 1.81 ± 0.99, respectively with no statistically significant difference among them ($p = 0.83$) (Fig. 2l). This result is consistent with the histopathology observation of very few inflammatory cells in FC. Greater pathology scores were determined for both TAF groups (TAF-UA_{hi} 10.19 ± 5.96; TAF-UA_{lo} 12.69 ± 3.66) with no statistically significant differences ($p = 0.96$) (Fig. 2m). This is attributable to the presence of inflammatory cells, necrosis, capsule thickness, and tissue infiltrate observed in most of the samples. Conversely, statistical significance was observed between TAF-UA_{lo} and PBS control ($p = 0.048$), and TAF-UA_{lo} and UA ($p = 0.039$). Notably, S_{pair} score for the UA group was negative (−1.06) indicating lower implant reactivity as compared to the PBS control group (Fig. 2m and n). S_{pair} scores for TAF-UA_{hi} (12.44) and TAF-UA_{lo} (16.88) instead indicated moderate and severe reactivity, respectively. Collectively, these results show that UA mitigated the FBR to implants with or without tissue exposure to TAF, in a concentration dependent manner. Notably however, UA lowered TAF solubility [11], which in turn reduced TAF release rate from the implant (Table 1).

It is therefore possible that the above observations may be due to the interplay of higher TAF and UA concentrations, rather than to UA alone. TAF produced an inflammatory response that could be clearly captured via both histopathology and measurements of local tissue thickening at the implantation site.

3.2. TAF PK in NHP

In conjunction with the analysis of subdermal tissue response to sustained TAF administration, TAF pharmacokinetics (PK) was investigated for three different TAF presentations: TAF_{fs}, TAF_{fb} or TAF-UA in rhesus macaques ($n = 4$/group). Based on the results obtained in the rat study, TAF-UA_{hi} (TAF:UA ratio 1:1) was chosen for this analysis. The three TAF presentations were constantly released for 3 months from the nanofluidic implants inserted subcutaneously in the animal dorsum. In a previous study in macaques, implants were shown to sustain constant TAF_{fs} release for 4 months [12]. TAF release rates from implants were calculated from drug residual in the implant reservoir after explanation. Similar daily release rates were observed for TAF_{fs} (1.40 ± 0.15 mg/day) and TAF_{fb} (1.36 ± 0.50 mg/day) groups (Table 2). For the TAF-UA group a lower daily release rate was measured (0.34 ± 0.10 mg/day), similar to the results obtained in rats.

Throughout the 3 months, all groups maintained similar intracellular tenofovir diphosphate (TFV-DP) concentration in peripheral blood mononuclear cells (PBMC). TFV-DP PBMC concentrations were 304 (IQR, 212.25 to 610.50) for TAF_{fs}, 381 (IQR, 191 to 1473) for TAF_{fb}, and 314 fmol/10^6 median (IQR, 168.25 to 601.50) for TAF-UA (Fig. 3a). Despite the significant difference in release rate achieved with the TAF-UA group as compared to TAF_{fs} and TAF_{fb}, no statistical difference was observed among groups.

Further, TAF plasma concentrations were a median 0.65 (IQR, 0.40 to 1.05 ng/mL), 0.79 (IQR, 0.48 to 0.99 ng/mL) and 0.54 (IQR, 0.41 to 0.74 ng/mL) for TAF_{fs}, TAF_{fb} and TAF-UA groups (Fig. 3b), respectively. Statistical significance was observed exclusively on day 14 between TAF_{fb} and TAF-UA groups ($p = 0.03$). In contrast, plasma TFV concentrations were 3.13 (IQR, 2.79 to 3.93 ng/mL), 4.98 (IQR, 3.77 to 6.89 ng/mL) and 3.24 (IQR, 2.50 to 4.39 ng/mL) for TAF_{fs}, TAF_{fb} and TAF-UA groups (Fig. 3c). Statistical significance was observed on day 14 between TAF_{fs} and TAF_{fb} group ($p = 0.03$). Observed PBMC and plasma concentrations for TAF fumarate group were consistent with our previous results [12], which confirmed implant release reproducibility.

Table 1
TAF release rates in rat nanofluidic devices.

Rat TAF implant group	Average TAF release rate (mg/day)
TAF-UA_{hi}	0.53 ± 0.34
TAF-UA_{lo}	1.26 ± 0.83

Table 2
TAF release rates in NHP nanofluidic devices.

NHP TAF implant group	Average TAF release rate (mg/day)
TAF_{fs}	1.40 ± 0.15
TAF_{fb}	1.36 ± 0.50
TAF-UA	0.34 ± 0.10

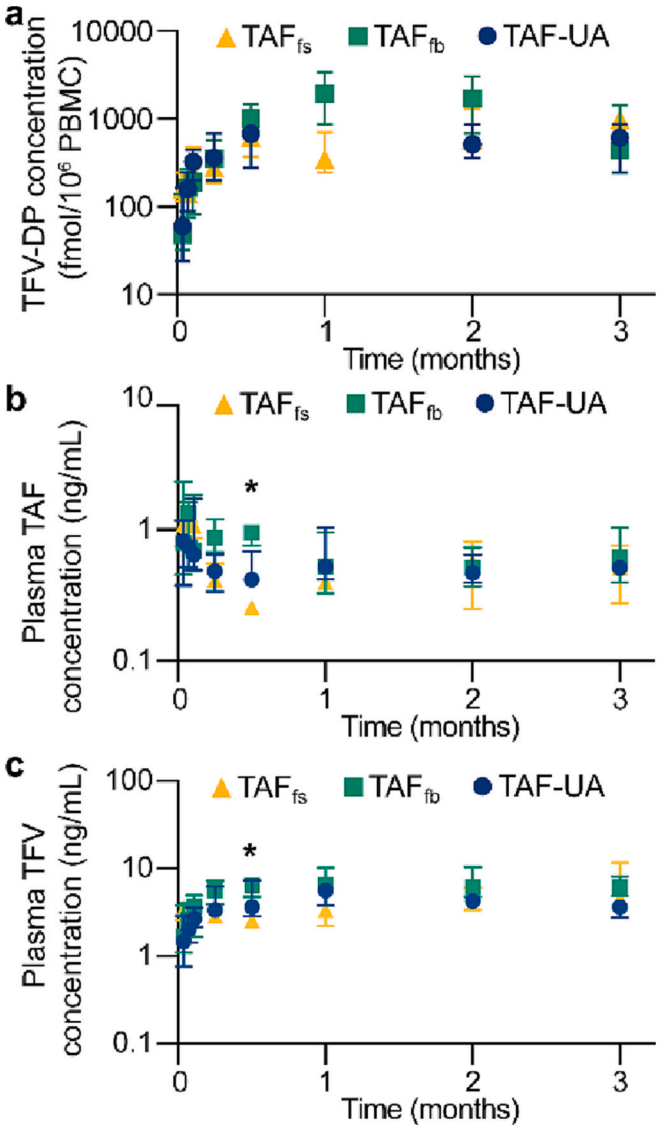

Fig. 3. Pharmacokinetics of TAF from NHP implanted with subcutaneous nanofluidic devices: TAF_{fs}, TAF_{fb} and TAF-UA. (a) Comparison of intracellular TFV-DP PBMC concentrations in 3 groups throughout the study. Evaluation of plasma (b) TAF and (c) TFV concentrations between 3 groups for the duration of the study. Data presented as median ± IQR.

3.3. Tolerability analysis for TAF-releasing subcutaneous implants in NHP

No deaths, serious adverse events (AE), or discontinuations due to an AE occurred throughout the study. Animal weight remained in the normal range and showed a steady growth consistent with healthy macaques (Supplementary Fig. S1). Systemic toxicity of subcutaneous

delivery of TAF_{fs} from nanofluidic implants was assessed in a previous study [12], where similar TAF release rates were achieved (mean 1.40 ± 0.39 mg/day) and sustained over 4 months. Specifically, due to TFV implication in nephrotoxicity and hepatotoxicity, kidney and liver function were previously assessed: creatinine and liver enzymes aspartate aminotransferase (AST) and alanine aminotransferase (ALT) were within the normal reference concentrations for rhesus macaques, with no variations noted throughout the study with respect to their baseline pre-implantation concentrations. Blood chemistry panel showed stable values within normal range for all TAF animals. Given the findings, we did not repeat these analyses in this study, which data is available in the previous publication [12].

To closely investigate the local tissue response and tolerability of sustained delivery of TAF, each animal served as its own control. For this, in addition to the TAF-loaded implant, each animal received a contralateral implant loaded with PBS, which served as no-drug control for analysis of tissues at implantation site. Clinical observations (Table 3) showed that implants were generally well tolerated (Fig. 4a–d). Of the 15 reported AEs, 12 were mild and 3 were moderate. Small scabs not procedure-related were noted over one PBS, one TAF_{fs} and one TAF-UA implant. Tissue induration was observed for 9 of 12 TAF-releasing implants. Specifically, 100%, 75%, and 50% of animals in the TAF-UA, TAF_{fb}, and TAF_{fs} groups, respectively showed tissue induration.

Changes in tissue thickness at implantation site (Supplementary Table S2) were measured as in the rat study (Fig. 4e). Mean $\Delta T_{x\text{-}y}$ values of −0.11 ± 0.29, 0.44 ± 0.89, 3.33 ± 3.59 and 3.18 ± 1.97 mm were observed over the 3 months study for control PBS, TAF_{fs}, TAF_{fb}, TAF-UA groups, respectively (Fig. 4f–j). Statistical significance was observed between the overall means of TAF_{fb} and PBS groups ($p = 0.019$), TAF-UA and PBS groups ($p = 0.0001$), and TAF-UA and TAF_{fs} groups ($p = 0.001$). Overall, a peak in $\Delta T_{x\text{-}y}$ was observed for all TAF groups between the 1st and 2nd week post-implantation, followed by a rapid decay toward steady $\Delta T_{x\text{-}y}$ levels, resolving by the 3rd week post-implantation. This transient swelling was particularly noticeable for implants in the TAF_{fb} group (Fig. 4h) and is consistent with an acute inflammation phase post-surgery. However, no changes in $\Delta T_{x\text{-}y}$ were noted for the PBS implants, which indicate that tissue swelling was exacerbated by the presence of the drug.

ΔT_z values for control PBS, TAF_{fs}, TAF_{fb}, and TAF-UA mean were 0.28 ± 0.21, 1.56 ± 0.65, 2.98 ± 1.55 and 3.90 ± 1.91 mm, respectively over 3 months (Fig. 4k–o). While no peak in swelling was observed orthogonally to the skin, all TAF groups displayed an early increase in tissue thickness along the z-axis, which remained consistent throughout the analysis. Statistical significance was observed between the overall means of PBS and TAF-UA groups ($p < 0.0001$) and TAF_{fs} and TAF-UA groups ($p = 0.0015$).

Collectively, assessment of swelling at implant site indicated that TAF_{fb} and TAF-UA implants were associated with highest level of tissue thickening while TAF_{fs} appeared to be better tolerated.

Table 3
NHP clinical observations of tolerability to TAF-releasing implants.

Adverse Events	PBS control n = 12 (%)	TAF_{fs} $n = 4$ (%)	TAF_{fb} $n = 4$ (%)	TAF-UA n = 4 (%)
General disorders				
Implant site erythema	1 (8.33)		1 (25)	1 (25)
Implant site induration		2 (50)	3 (75)	4# (100)
Implant site pruritus	1* (8.33)	1* (25)		1* (25)
Implant site hematoma				
Procedure complication				
Wound complication				
Wound secretion				

Footnote: All adverse events are mild, unless otherwise states. # means 3 out of 4 were moderate, * signifies a small scab was noted.

3.4. Local changes in tissue microenvironment from sustained subcutaneous TAF release

Two board-certified pathologists independently and blindly scored the fibrotic tissue directly in contact with the implant to assess foreign-body reaction and tolerability. Complete histological cross-sections of FC (H&E) are shown in Fig. 5a–d for each implant group, together with respective magnified areas of interests (Fig. 5e–h). Total histological scores were TAF_{fs} (14.50 ± 3.54), TAF_{fb} (15.75 ± 2.06) and TAF-UA (16.88 ± 2.59) (Fig. 5i and k), with no statistical difference among groups. Similar histological findings were observed in all three TAF-releasing groups, inflammatory cells, necrosis, capsule thickness, and tissue infiltrate (Supplementary Table S3). While higher scores for lymphocytes and plasma cells were noted for the TAF-UA group, more signs of necrosis were identified in the TAF_{fb} group. Tissue infiltrate was scored similarly in TAF-UA and TAF_{fb} groups. All TAF-releasing groups had same score in macrophage quantification. Statistical difference was observed between the three TAF groups and control PBS: TAF fumarate ($p = 0.0065$), TAF ($p = 0.0005$) and TAF-UA ($p = 0.013$). All 3 TAF groups received an average placebo-adjusted implant reactivity score (S_{pair}) that classified them as severe reaction ($15.1 \leq S_{pair} \leq 40$): TAF fumarate (18.07), TAF (20.57) and TAF-UA (20.32) (Fig. 5j and k).

The FCs in contact with implants were further assessed in terms of thickness (Fig. 5l), collagen density (Fig. 5m), and blood vessel count (Fig. 5n), focusing on tissues adjacent to the membrane or located on the opposite side of implants. Fibrotic capsules were significantly thicker in TAF groups than in PBS control (Fig. 5l). Thicknesses (mean ± SD) were: 241.27 ± 89.76 μm (PBS), 1511.32 ± 414.087 μm (TAF_{fs}), 1579.62 ± 862.12 μm (TAF_{fb}), and 1523.84 ± 370.11 μm (TAF-UA). Statistical significance in FC thickness was observed between PBS group with TAF_{fs} ($p < 0.0001$), TAF_{fb} ($p < 0.0001$) and TAF-UA ($p < 0.0001$). Notably, for all groups FC in contact with the nanofluidic membrane was significantly thicker than on the opposite implant side. Thicknesses (mean ± SD) on the opposite implant side and p-values with respect to tissue thickness adjacent to the membrane were: 145.44 ± 60.88 μm (PBS, $p < 0.0001$), 492.65 ± 267.31 μm (TAF_{fs}, $p < 0.0001$), 468.2 ± 279.41 μm (TAF_{fb}, $p < 0.0001$), and 805.01 ± 284.6 μm (TAF-UA, $p < 0.0001$). For TAF groups, constant local drug exposure causes chronic inflammation in proximity to the membrane, which leads to thickening of FC. In this context, mean TFV-DP concentration in FC in contact with the membrane were 110.3 (SD, ± 47.5 fmol/mg), 377.6 (SD, ± 385.8 fmol/mg) and 437 (SD, ± 303.6) for TAF_{fs}, TAF_{fb} and TAF-UA, respectively, with no statistical difference between groups (Fig. 5m). For PBS implants, the slight increase in FC may be attributed to shear stress in correspondence of the drug outlets, which create a morphological discontinuity in the implant surface, not present on the opposite side of implants.

Masson Trichrome staining did not show significant differences in collagen density (mean ± SD, %) in FCs among groups (Fig. 5n). Collagen density adjacent to the membrane was: PBS (3.64 ± 2.48), TAF_{fs} (4.08 ± 1.28), TAF_{fb} (5.96 ± 3.45) and TAF-UA (3.80 ± 2.22) (Fig. 5n). For each group, collagen density was also similar for tissues on the opposite side of membranes with no statistical significance between the two sides: PBS (4.04 ± 1.91, $p = 0.99$), TAF_{fs} (4.58 ± 3.97), TAF_{fb} (3.93 ± 1.61). Statistical difference was only observed for the TAF-UA group (5.77 ± 1.65, $p = 0.030$).

Foreign-body response begins as a pro-inflammatory state and stimulates angiogenesis to increase transportation of inflammatory cells and cytokines [24,25]. Angiogenesis was quantified via count of blood vessel lumens in FCs (Fig. 5o). No statistically significant differences were observed among groups and between FC close to membrane or

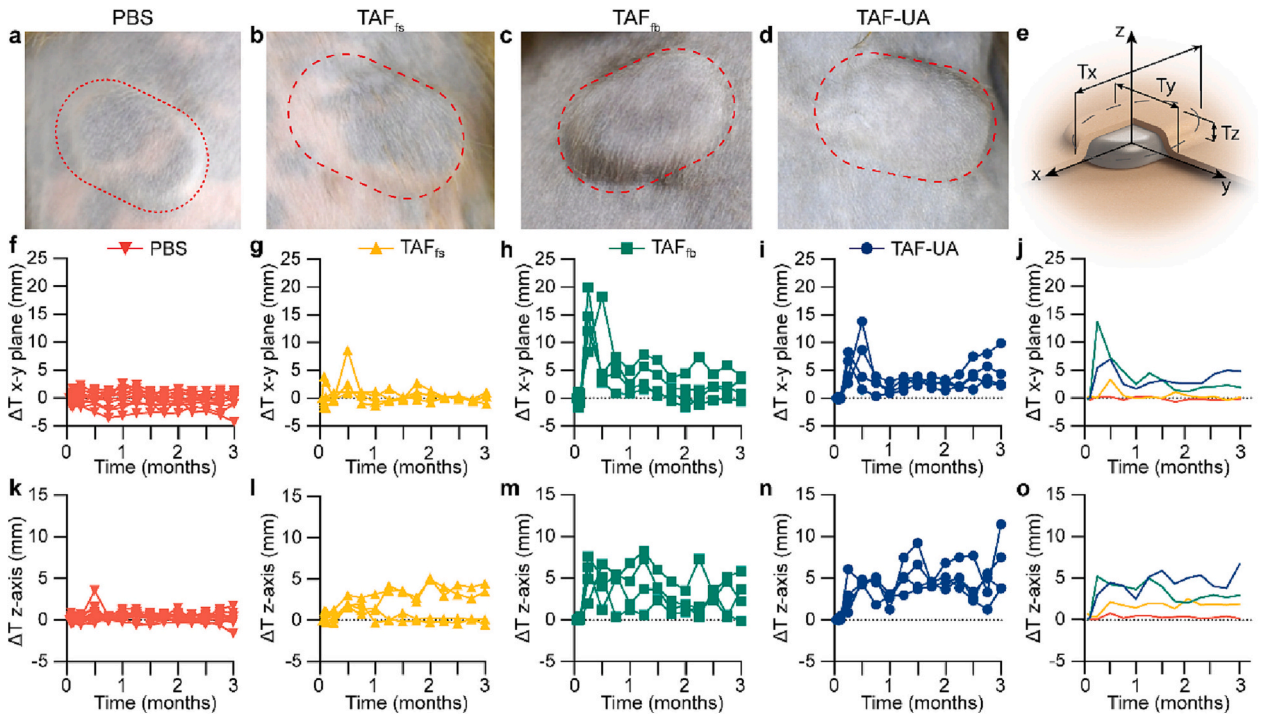

Fig. 4. Comparison of safety and tolerability of TAF-releasing nanofluidic devices in NHP. Representative images of (a) PBS, (b) TAF_{fs}, (c) TAF_{fb} and (d) TAF-UA implants in NHP at 3 months. (e) Schematics of a subcutaneous implant illustrating the measurements of tissue thickness along the x-, y- and z-axes. Longitudinal changes in implant thickness ($\Delta T_{x\text{-}y}$) averaged with respect to length and width (x-y plane) over 3 months for implants loaded with (f) PBS, (g) TAF_{fs}, (h) TAF_{fb}, (i) TAF-UA, and (j) comparison of 4 groups. Change in implantation site thickness along the z-axis (ΔT_z) throughout 3 months in (k) PBS, (l) TAF_{fs}, (m) TAF_{fb}, (n) TAF-UA, and (o) comparison of the 4 groups.

opposite implant side. For reference, the number of blood vessel lumens (mean ± SD, count) in FCs in contact with membrane were: PBS (10.09 ± 6.70), TAF_{fs} (28.5 ± 29.44), TAF_{fb} (35 ± 28.89) and TAF-UA (43 ± 53.14). However, significant variability in blood vessel count was noted in correspondence to the membrane, which is consistent with the results obtained in rats.

Overall, these results demonstrate that all forms of TAF generated a chronic inflammatory response in a concentration dependent manner. However, this had no visible effect on collagen density and angiogenesis in FC, which are relevant factor in local drug diffusion and permeation in systemic circulation. In this context, to evaluate whether the FC would limit drug release and systemic delivery, we performed FRAP to quantify differences among groups in the effective diffusivity of fluorescein isothiocyanate (FITC) in the fibrotic tissues. FITC was used as a fluorescent surrogate for TAF due to similar molecular weight and water solubility. Mean effective diffusivities were $3.08 \pm 0.19 \times 10^{-7}$ cm^2/s for PBS, $3.55 \pm 0.13 \times 10^{-7}$ cm^2/s for TAF_{fs}, $3.58 \pm 0.54 \times 10^{-7}$ cm^2/s for TAF_{fb}, and 3.28, ± 0.14 × 10^{-7} cm^2/s for TAF-UA (Fig. 5p). These values are similar to FITC effective diffusivity in subcutaneous tissues ($3.45 \pm 0.33 \times 10^{-7}$ cm^2/s). No statistical difference was observed between PBS, TAF groups and subcutaneous tissues, indicating that the FC does not generate an impediment to TAF release. These findings are also consistent with the PK results, where no inflection in PK was observed longitudinally due to the progressive formation of fibrotic tissue around the implants.

To further characterize the difference in local inflammatory response between PBS and TAF groups, sections of FCs with marked inflammation and immune infiltration were selected for imaging mass cytometry (IMC) analysis. As such, IMC results are reflective of the highest level of FBR observed for PBS (Fig. 5q), TAF_{fs} (Fig. 5r), TAF_{fb} (Fig. 5s) and TAF-UA (Fig. 5t) and not meant to be representative of the average tissue response across complete FC sections, which was milder. PBS-loaded implant control showed negligible immune infiltration, and mild activation of Th1 cells (population 12), which is consistent with bioinert implantable devices. Common to all TAF groups as compared to PBS controls, there was higher influx of activated immune cells to the FC, with clear increase in number of granzyme B+ neutrophils (population 18, 19). Higher presence of activated immunosuppressive regulatory T cells in proliferative state, namely CD45 + CD3 + Foxp3 + PD-1 + Ki67+ cells (population 10) was also observed across all TAF groups. However, notably TAF_{fb} presented the lowest level of immune infiltration, displaying similar t-SNE plot as PBS control. Both TAF_{fs} and TAF_{UA} presented higher level of immune response, with marked presence of exhausted cytotoxic CD45 + CD3 + CD8+ T cells (population 8, 11) and broader distribution of immunosuppressive T regs, indicative of an immune response to a sustained local perturbation of the microenvironment. Additionally, higher M2 polarized macrophage infiltration (populations 1, 2, 4) was observed for TAF_{fs}, indicating a wound healing response. In contrast, TAF_{fb} and TAF-UA portray higher M1 polarized macrophage infiltration with production of inflammatory cytokines and chemokines (populations 5, 6). Further, significant increase in activated CD45 + CD20 + HLA-DR+ B cells (population 7) denoted the stimulation of an adaptive immune response in TAF_{UA} samples. Overall, the response in the TAF samples in contact with the TAF-releasing membrane is in a constant state of pro- and anti-inflammation likely attributable to constant drug exposure.

4. Discussion

In this study we performed a comparative assessment of the tolerability and tissue response of sustained subcutaneous administration of three forms of TAF released from a nanofluidic implant.

The analysis was performed in Sprague Dawley rats and rhesus macaques, which species offered differences rendering them both suitable to assess different aspects of tolerability and foreign body response (FBR) to subdermal long-acting antiretroviral delivery implants.

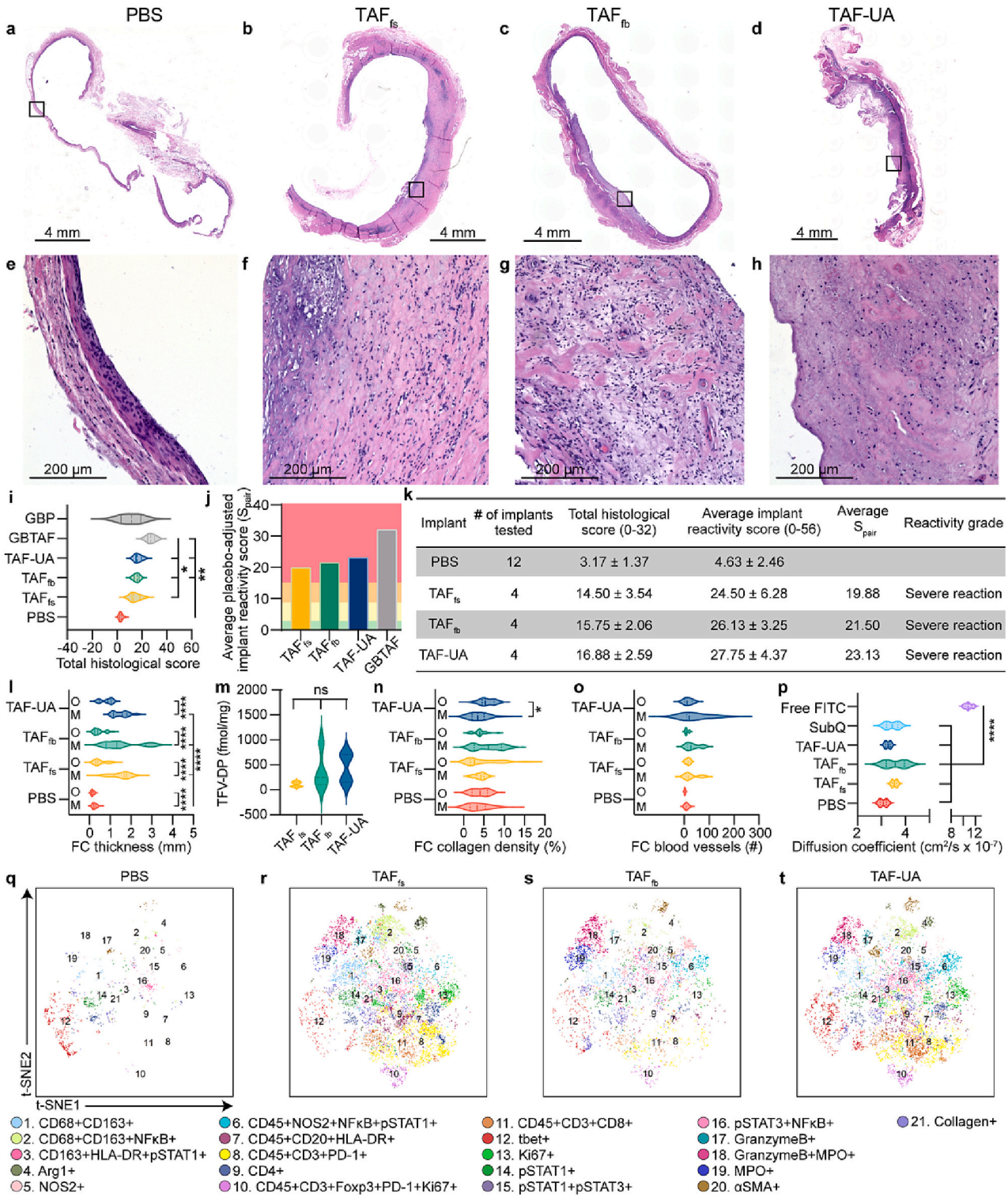

Implant	# of implants tested	Total histological score (0-32)	Average implant reactivity score (0-56)	Average S_{pair}	Reactivity grade
PBS	12	3.17 ± 1.37	4.63 ± 2.46		
TAF_{fs}	4	14.50 ± 3.54	24.50 ± 6.28	19.88	Severe reaction
TAF_{fb}	4	15.75 ± 2.06	26.13 ± 3.25	21.50	Severe reaction
TAF-UA	4	16.88 ± 2.59	27.75 ± 4.37	23.13	Severe reaction

Fig. 5. H&E staining of 3-month fibrotic capsule (FC) in (a) PBS, (b) TAF_{fs}, (c) TAF_{fb} and (d) TAF-UA, and respective magnifications (e–h). (i) Evaluation of total histological scores between PBS, TAF_{fs}, TAF_{fb} and TAF-UA groups in comparison to Generation B (GB) TAF and placebo implants from Su et al. [15] (j) Assessment of average S_{pair} reactivity grade between TAF_{fs}, TAF_{fb}, TAF-UA in comparison to GB TAF implants. S_{pair} values: 0.0–2.9 green colour (no reaction), 3.0–8.9 yellow (slight reaction), 9.0–15.0 orange (moderate reaction), and > 15.1 red (severe reaction). (k) Table with histopathological scoring in all 4 groups. Data presented as mean ± SD. Comparison of (l) FC thickness, (m) collagen percentage in FC area, (n) blood vessel quantity in FC and (o) FRAP diffusivity coefficient between PBS and TAF nanofluidic implant groups. Free FITC diffusivity ($1.09 \pm 0.06 \times 10^{-6}$ cm^2/s) is reported as reference value. (p) TFV-DP concentration in FC adjacent to membranes. Imaging Mass Cytometry (IMC) t-SNE plots for representative FC samples (q) PBS, (r) TAF_{fs}, (s) TAF_{fb}, and (t) TAF-UA. (For interpretation of the references to colour in this figure legend, the reader is referred to the web version of this article.)

NHP have an immune system that is more similar to humans than rats, which affects the FBR to implants and clinical translatability of results. In this context, differences exist in the population of immune cells [26] and their function. For example, NHP macrophages are more similar to those from humans in their ability to phagocytize and clear debris [27]. In addition, NHP have a more complex major histocompatibility complex system, which allows for a more diverse and specific immune response. Rats have a stronger and more rapid inflammatory response than NHP, which is mainly driven by macrophages and neutrophils [28]. This can lead to more severe tissue damage and the formation of a thick fibrotic capsule around the implant [28], as noted in our study. In contrast, NHP have a more controlled and gradual inflammatory response, mainly driven by macrophages and foreign body giant cells, which results in a thinner and more fibrous capsule around an implant [29]. Rats and NHPs also differ in the types and amount of cytokines they produce in response to foreign materials [30]. Finally, NHP exhibit more complex behaviors than rats, which renders them better suited for studying the long-term effects and tolerability of subdermal implants, including how potential discomfort may impact behavior [31].

For the analysis, the three formulations used were TAF_{fs}, TAF_{fb} and TAF_{fb} with urocanic acid (TAF-UA). TAF quickly hydrolyzes to TFV^4, greatly impairing the stability of TAF needed for long-term implant drug delivery. We previously addressed this problem with the addition of *trans*-urocanic acid, which showed to significantly slow TAF degradation in vivo [11].

Beside its use as a TAF-stabilizing excipient, UA is known to possess immunosuppressive properties. *Trans*-UA is endogenous in the skin, and it isomerizes to *cis*-UA upon absorption of UV-B radiation. *Cis*-UA interacts with skin fibroblasts, which alter the function of antigen-presenting cells (APCs), ultimately activating suppressor T cells [32]. Our rat study showed that increasing concentrations of *trans*-UA mildly mitigated inflammation from sustained tissue exposure to TAF [33]. Although there was no statistical significance in the histological scoring between both TAF-UA groups, there was a difference in implant reactivity grade. The TAF-UA_{hi} group had an S_{pair} score of 10.38 compared to TAF-UA_{lo} score of 16.75, corresponding to moderate and severe reactivity, respectively. These results informed our choice of TAF-UA_{hi} for the study in NHP. The negative S_{pair} scoring obtained for the UA-implant group provided additional support for UA ability to mitigate FBR.

To assess the PK of the three TAF presentations, in the NHP study we quantified and compared TAF and TFV plasma concentrations and TFV-DP PBMC intracellular concentration among groups. We expected UA to maintain higher TAF stability in the implant as compared to TAF_{fs} and TAF_{fb}. In the latter groups a higher level of TAF hydrolyzation into TFV was expected to occur prior to release from implants. Upon subcutaneous delivery, TAF or TFV enter systemic circulation and reach the PBMC. TAF passively enters PBMC at a faster rate than TFV^4. Within cells, TAF is hydrolyzed to TFV and TFV is phosphorylated to the pharmacologically active TFV-DP. Although the release rate in the TAF-UA group was approximately half of that measured for TAF_{fs} and TAF_{fb}, similar TFV-DP concentrations were observed in PBMC. This finding supports the hypothesis that UA provided TAF-stabilization and TAF-UA implants released a higher percentage of intact TAF as compared to TAF_{fs} and TAF_{fb} implants, resulting in better PBMC delivery efficiency. For reference, all three TAF implant groups showed significantly lower TFV plasma concentrations as compared to macaques receiving oral TAF at approximately one quarter of the dose [34]. Given TFV nephrotoxicity and effect on loss of bone mineral density [4], the reduction of TFV plasma concentrations represents an advantage of LA subdermal TAF systems over oral administration.

The analysis of local tissue response showed that all TAF presentations generated a foreign body response that was significantly more pronounced than that for control PBS implants. This was consistent between rats and non-human primates. In NHP, upon resolution of an acute inflammation phase during the first two weeks post-implantation, marked by a peak in $\Delta T_{x\text{-}y}$ (Fig. 4f-j), all groups achieved a state of TAF-related chronic inflammation with variable levels of tissue swelling at implantation site. These results are consistent with our previous findings [12], albeit in the earlier study a milder tissue response was observed. Our results are also consistent with reports from other groups [15,33,35]. It is worth noting, however, that despite higher TAF release rates achieved in the present study, no ulcerations or significant AE at the site of implantation were observed, in contrast to previous reports. As an example, for all TAF groups, reactivity scores were 10 points lower than the S_{pair} scores (32.0) achieved for the GB TAF implant reported by Su et al. [15] Similar differences were observed in total histological scores. These differences can be partly due to implant materials, size, shape, and surface physicochemical properties, which alone are known to affect FBR to implantable devices [24].

Histological analysis of tissues surrounding the implants showed one order of magnitude thicker FC as compared to PBS control. TAF exposure had a milder effect on FC composition: differences in collagen density and blood vessel lumen count for TAF compared to PBS control were limited and more pronounced in rats than in NHP. Specific differences in collagen density could be ascribed to TAF-induced metalloprotease tissue degradation. The increased number of blood vessels as compared to the PBS control could be attributed to inflammation-induced angiogenesis. Notably, no significant differences were observed in FITC effective diffusivity in FC tissues among TAF groups and PBS control and subcutaneous tissue, indicating that the fibrotic tissue encapsulating implants does not impair interstitial transport and systemic delivery of small molecules such as TAF.

Our study also aimed at further characterizing immune cell infiltration in the tissues surrounding TAF implants. All three TAF groups exhibited cell populations indicative of active chronic inflammation and simultaneous counter anti-inflammation response attributable to constant TAF exposure. We posit that chronic TAF exposure stimulate the recruitment of inflammatory cells on site, but the lack of antigens impedes immune activation.

Notably, drug release directionality offered by our nanofluidic implants allowed us to observe differential tissue response at different levels of TAF exposure. Statistically thicker FCs were reported near the nanofluidic membrane than on the opposite side of implants. Chronic inflammation was limited to FC adjacent to membrane. Our findings may partially explain why implants with a larger drug release surface area exhibited more severe AE (including necrosis and ulceration) [15,33,35] as compared to our implants. A key finding was that for drugs eliciting an inflammatory tissue response, release direction with respect to the body can determine implant tolerability or rejection. Further support for this observation was previously obtained by our group with sustained subdermal delivery of the nucleoside reverse transcriptase translocation inhibitor islatravir. Islatravir was well tolerated when its release was directed toward the subcutaneous tissues [6]. Conversely islatravir produced acute inflammation, tissue necrosis, and ulceration when released toward the skin. We posit that small molecule drug clearance from sustained subdermal elution is more effective when drug is released in proximity to the dermal-subcutaneous junction as opposed to directed toward the epidermis. The dermal-subcutaneous junction contains the lower vascular plexus that supplies to arterioles that connect with the systemic circulatory system. The epidermis is avascular and receives nutrients via diffusion from upper vascular plexus located between the papillary and reticular dermis [36,37]. Therefore, drug that is released toward the epidermis is 'cleared' by the upper plexus and accumulates near the epidermis. Moreover, higher drug concentration constantly triggers inflammation, which activate metalloproteases that lyse extracellular matrix [38]. External insults such as friction and mechanical stress near the implant, coupled with the continuous internal insults could lead to skin ulceration. To date, most LA delivery implants control drug delivery through polymeric membranes or degradable polymeric structures and do not offer release directionality [15,39]. Our observation may guide the development of next generation LA drug

delivery systems.

5. Conclusions

Contrasting results have been reported regarding local tissue tolerability of sustained subdermal TAF administration. However, these studies involved different TAF formulations and delivery systems. Here we performed a systematic analysis of FBR to sustained TAF delivery using three TAF presentations released from bioinert subcutaneous nanofluidic implants. Overall, our results indicate that all three TAF presentations produced a concentration-dependent chronic inflammatory response in the tissue surrounding the implants. UA appeared to enhance TAF delivery to PBMC by maintaining TAF stability within the implant but its immunomodulatory effect in tissue surrounding implants was limited and exclusively observed in the rat study. In fact, in rhesus macaques IMC and histopathology results for TAF_{fb} and TAF_{fs} showed milder FBR as compared to TAF-UA, despite higher delivery rates. Collectively, the results were consistent in rats and non-human primates. However, their clinical translatability and final determination of tolerability of TAF subdermal delivery will require direct clinical investigation. In this context, the CAPRISA clinical study is expected to provide highly relevant results.

Funding

This work was supported by Gilead Sciences, funding from the National Institutes of Health National Institute of Allergy and Infectious Diseases (R01AI120749; A.G.), and the National Institutes of Health National Institute of General Medical Sciences (R01GM127558; A.G.). A. G. is an inventor of intellectual property licensed by Semper Therapeutics. A.G. and P.L.A. receives grants and contracts from Gilead Sciences paid to their respective institutions. A.G. does not perform consulting activities. P.L.A. collects personal fees from Gilead Sciences. All other authors declare that they have no competing interests or consulting engagements.

CRediT authorship contribution statement

Fernanda P. Pons-Faudoa: Conceptualization, Data curation, Formal analysis, Investigation, Project administration, Visualization, Writing – original draft, Writing – review & editing. **Nicola Di Trani:** Formal analysis, Investigation, Visualization, Writing – review & editing. **Simone Capuani:** Formal analysis, Investigation, Visualization, Writing – review & editing. **Nathanael Hernandez:** Investigation. **Anthony M. Wood:** Investigation. **Bharti Nehete:** Investigation. **Jean Niles:** Investigation. **Kathryn A. Shelton:** Investigation. **Sarah Kezar:** Investigation. **Lane R. Bushman:** Investigation, Methodology, Validation. **Corrine Ying Xuan Chua:** Writing – original draft, Writing – review & editing. **Michael M. Ittmann:** Investigation. **Peter L. Anderson:** Methodology, Resources, Validation, Writing – review & editing. **Pramod N. Nehete:** Investigation, Project administration, Resources, Writing – review & editing. **Roberto C. Arduino:** Conceptualization, Writing – review & editing. **Joan E. Nichols:** Conceptualization, Investigation, Visualization, Writing – review & editing. **Alessandro Grattoni:** Conceptualization, Funding acquisition, Investigation, Project administration, Resources, Supervision, Visualization, Writing – original draft, Writing – review & editing.

Data availability

Data will be made available on request.

Acknowledgements

We thank Dr. Andreana L. Rivera, Yuelan Ren, and Sandra Steptoe from the research pathology core of Houston Methodist Research Institute. We thank Luke Segura, Dana Salazar, Matthew McAdams and Elizabeth Lindemann from the Michale E. Keeling Center for Comparative medicine and Research at UTMDACC for support in animal studies. We thank Jim Rooney, Michael Clarke, Rich Clark, Chelsea Snyder, Bhanu Singh, and Christian Callebaut from Gilead Sciences for helpful insight and discussions.

Appendix A. Supplementary data

Supplementary data to this article can be found online at https://doi.org/10.1016/j.jconrel.2023.04.037.

References

[1] UNAIDS, Miles to Go: Global AIDS Update 2018, 2018, p. 59 [pdf].
[2] R.M. Grant, et al., Uptake of pre-exposure prophylaxis, sexual practices, and HIV incidence in men and transgender women who have sex with men: a cohort study, Lancet Infect. Dis. 14 (2014) 820–829, https://doi.org/10.1016/S1473-3099(14)70847-3.
[3] J.M. Baeten, et al., Antiretroviral prophylaxis for HIV prevention in heterosexual men and women, New Engl. J. Med. 367 (2012) 399–410, https://doi.org/10.1056/NEJMoa1108524.
[4] A.S. Ray, M.W. Fordyce, M.J. Hitchcock, Tenofovir alafenamide: a novel prodrug of tenofovir for the treatment of human immunodeficiency virus, Antivir. Res. 125 (2016) 63–70.
[5] C.Y.X. Chua, et al., Transcutaneously refillable nanofluidic implant achieves sustained level of tenofovir diphosphate for HIV pre-exposure prophylaxis, J. Control. Release 286 (2018) 315–325, https://doi.org/10.1016/j.jconrel.2018.08.010.
[6] F.P. Pons-Faudoa, et al., Ultra-long-acting refillable nanofluidic implant confers full protection against SHIV infection in non-human primates, bioRxiv (2022), https://doi.org/10.1101/2022.12.15.520646, 2022.2012.2015.520646.
[7] F.P. Pons-Faudoa, et al., 2-Hydroxypropyl-β-cyclodextrin-enhanced pharmacokinetics of cabotegravir from a nanofluidic implant for HIV pre-exposure prophylaxis, J. Control. Release 306 (2019) 89–96, https://doi.org/10.1016/j.jconrel.2019.05.037.
[8] F.P. Pons-Faudoa, A. Ballerini, J. Sakamoto, A. Grattoni, Advanced implantable drug delivery technologies: transforming the clinical landscape of therapeutics for chronic diseases, Biomed. Microdevices 21 (2019) 47, https://doi.org/10.1007/s10544-019-0389-6.
[9] C. Flexner, Antiretroviral implants for treatment and prevention of HIV infection, Curr. Opin. HIV AIDS 13 (2018) 374–380, https://doi.org/10.1097/coh.0000000000000470.
[10] T.N. Gengiah, et al., CAPRISA 018: a phase I/II clinical trial study protocol to assess the safety, acceptability, tolerability and pharmacokinetics of a sustained-release tenofovir alafenamide subdermal implant for HIV prevention in women, BMJ Open 12 (2022), https://doi.org/10.1136/bmjopen-2021-052880 e052880.
[11] A. Sizovs, et al., Trans-urocanic acid enhances tenofovir alafenamide stability for long-acting HIV applications, Int. J. Pharm. 587 (2020) 119623, https://doi.org/10.1016/j.ijpharm.2020.119623.
[12] F.P. Pons-Faudoa, et al., Preventive efficacy of a tenofovir alafenamide fumarate nanofluidic implant in SHIV-challenged nonhuman primates, Adv. Ther. 4 (2021) 2000163, https://doi.org/10.1002/adtp.202000163.
[13] N. Di Trani, et al., Extending drug release from implants via transcutaneous refilling with solid therapeutics, Adv. Ther. 2100214 (2021), https://doi.org/10.1002/adtp.202100214 **n/a**.
[14] F.P. Pons-Faudoa, et al., Viral load reduction in SHIV-positive nonhuman primates via long-acting subcutaneous tenofovir alafenamide fumarate release from a nanofluidic implant, Pharmaceutics 12 (2020) 981.
[15] J.T. Su, et al., A subcutaneous implant of tenofovir alafenamide fumarate causes local inflammation and tissue necrosis in rabbits and macaques, Antimicrob. Agents Chemother. 64 (2020), https://doi.org/10.1128/AAC.01893-19.
[16] Standardization, W. H. O. E. C. o. B. & Organization, W. H, WHO Expert Committee on Biological Standardization: Sixty-Sixth Report 999, World Health Organization, 2016.
[17] J.C.G. Blonk, A. Don, H. Van Aalst, J.J. Birmingham, Fluorescence photobleaching recovery in the confocal scanning light microscope, J. Microsc. 169 (1993) 363–374, https://doi.org/10.1111/j.1365-2818.1993.tb03312.x.
[18] H.-C. Liu, et al., Potentiating antitumor efficacy through radiation and sustained Intratumoral delivery of anti-CD40 and anti-PDL1, Int. J. Radiat. Oncol. Biol. Phys. (2020), https://doi.org/10.1016/j.ijrobp.2020.07.2326.
[19] D. Schapiro, et al., histoCAT: analysis of cell phenotypes and interactions in multiplex image cytometry data, Nat. Methods 14 (2017) 873–876, https://doi.org/10.1038/nmeth.4391.
[20] L.R. Bushman, et al., Determination of nucleoside analog mono-, di-, and triphosphates in cellular matrix by solid phase extraction and ultra-sensitive LC–MS/MS detection, J. Pharm. Biomed. Anal. 56 (2011) 390–401.
[21] P.L. Anderson, et al., Emtricitabine-Tenofovir Concentrations and Pre-Exposure Prophylaxis Efficacy in Men Who have Sex with Men, 1946–6242 (Electronic) 1946–6234 (Linking), 2012.

[22] P.H. Hart, M. Norval, The multiple roles of urocanic acid in health and disease, J. Investig. Dermatol. 141 (2021) 496–502, https://doi.org/10.1016/j.jid.2020.07.017.
[23] S. Gruner, W. Diezel, H. Stoppe, H. Oesterwitz, W. Henke, Inhibition of skin allograft rejection and acute graft-versus-host disease by cis-urocanic acid, J. Investig. Dermatol. 98 (1992) 459–462, https://doi.org/10.1111/1523-1747.ep12499855.
[24] S. Capuani, G. Malgir, C.Y.X. Chua, A. Grattoni, Advanced strategies to thwart foreign body response to implantable devices, Bioeng. Transl. Med. e10300 (2022).
[25] A.W. Ho, T.S. Kupper, T cells and the skin: from protective immunity to inflammatory skin disorders, Nat. Rev. Immunol. 19 (2019) 490–502, https://doi.org/10.1038/s41577-019-0162-3.
[26] K.A. Phillips, et al., Why primate models matter, Am. J. Primatol. 76 (2014) 801–827.
[27] J.L. Flynn, H.P. Gideon, J.T. Mattila, P.L. Lin, Immunology studies in non-human primate models of tuberculosis, Immunol. Rev. 264 (2015) 60–73.
[28] W.K. Ward, A review of the foreign-body response to subcutaneously-implanted devices: the role of macrophages and cytokines in biofouling and fibrosis, J. Diabetes Sci. Technol. 2 (2008) 768–777.
[29] J.C. Doloff, et al., Colony stimulating factor-1 receptor is a central component of the foreign body response to biomaterial implants in rodents and non-human primates, Nat. Mater. 16 (2017) 671–680.
[30] I. Messaoudi, R. Estep, B. Robinson, S.W. Wong, Nonhuman primate models of human immunology, Antioxid. Redox Signal. 14 (2011) 261–273.
[31] W.R. Hein, P.J. Griebel, A road less travelled: large animal models in immunological research, Nat. Rev. Immunol. 3 (2003) 79–84.
[32] F.P. Noonan, E.C. De Fabo, Immunosuppression by ultraviolet B radiation: initiation by urocanic acid, Immunol. Today 13 (1992) 250–254, https://doi.org/10.1016/0167-5699(92)90005-R.
[33] J.W. Romano, et al., Tenofovir alafenamide for HIV prevention: review of the proceedings from the gates foundation long-acting TAF product development meeting, AIDS Res. Hum. Retrovir. 37 (2021) 409–420, https://doi.org/10.1089/aid.2021.0028.
[34] I. Massud, et al., Efficacy of oral tenofovir alafenamide/emtricitabine combination or single-agent tenofovir alafenamide against vaginal simian human immunodeficiency virus infection in macaques, J. Infect. Dis. 220 (2019) 1826–1833, https://doi.org/10.1093/infdis/jiz383.
[35] M. Mascolini, Biodegradable TAF Implants Protect 6 of 6 Macaques From Vaginal SHIV, HIV 4RP, 2021.
[36] M. Friedel, et al., Opportunities and challenges in the diagnostic utility of dermal interstitial fluid, Nat. Biomed. Eng. 1-15 (2023).
[37] K. Kretsos, G. Kasting, Dermal capillary clearance: physiology and modeling, Skin Pharmacol. Physiol. 18 (2005) 55–74.
[38] L. Guenin-Macé, R. Oldenburg, F. Chrétien, C. Demangel, Pathogenesis of skin ulcers: lessons from the mycobacterium ulcerans and Leishmania spp. pathogens, Cell. Mol. Life Sci. 71 (2014) 2443–2450.
[39] L.M. Johnson, et al., Characterization of a reservoir-style implant for sustained release of tenofovir alafenamide (TAF) for HIV pre-exposure prophylaxis (PrEP), Pharmaceutics 11 (2019) 315, https://doi.org/10.3390/pharmaceutics11070315.